Hindawi
Complexity
Volume 2019, Article ID 5367403, 11 pages
https://doi.org/10.1155/2019/5367403

Research Article

An Optimal Allocation Strategy for Multienergy Networks Based on Double-Layer Nondominated Sorting Genetic Algorithms

Min Mou, Da Lin, Yuhao Zhou, Wenguang Zheng, Jiongming Ruan, and Dongdong Ke

Huadian Electric Power Research Institute Co., Ltd., Hangzhou, Zhejiang 310013, China

Correspondence should be addressed to Min Mou; min-mou@chder.com

Received 26 July 2019; Accepted 4 September 2019; Published 29 October 2019

Guest Editor: Xiaoqing Bai

Aiming at the problems of complex structures, variable loads, and fluctuation of power outputs of multienergy networks, this paper proposes an optimal allocation strategy of multienergy networks based on the double-layer nondominated sorting genetic algorithm, which can optimize the allocation of distributed generation (DG) and then improve the system economy. In this strategy, the multiobjective nondominated sorting genetic algorithm is adopted in both layers, and the second-layer optimization is based on the optimization result of the first layer. The first layer is based on the structure and load of the multienergy network. With the purpose of minimizing the active power loss and the node voltage offset, an optimization model of the multienergy network is established, which uses the multiobjective nondominated sorting genetic algorithm to solve the installation location and the capacity of DGs in multienergy networks. In the second layer, according to the optimization results of the first layer and the characteristics of different DGs (wind power generator, photovoltaic panel, microturbine, and storage battery), the optimization model of the multienergy network is established to improve the economy, reliability, and environmental benefits of multienergy networks. It uses the multiobjective nondominated sorting genetic algorithm to solve the allocation capacity of different DGs so as to solve the optimal allocation problem of node capacity in multienergy networks. The double-layer optimization strategy proposed in this paper greatly promotes the development of multienergy networks and provides effective guidance for the optimal allocation and reliable operation of multienergy networks.

1. Introduction

Energy is the driving force and foundation for social and economic development. As traditional fossil energy sources are increasingly exhausted, improving energy efficiency, developing new energy sources, and strengthening multienergy complementarity have become inevitable choices to solve the contradiction between energy demand growth and energy shortage in the process of social and economic development. The multienergy network is a hybrid energy supply system that integrates multiple DGs, energy storage units, loads, and monitoring and protection devices. It can be flexibly connected to the grid or operated on isolated islands, which can effectively improve the flexibility, economy, and cleanliness of power system operation, and meet the requirements of users for power supply reliability, safety, and power quality. Since wind resources and solar resources are clean energy, the power generation of the micro gas turbine (MT) is stable and controllable, and the battery can suppress system power fluctuations. The node diagram of a typical multienergy network is shown in Figure 1. Therefore, the multienergy network studied in this paper includes a wind turbine generator (WTG), a photovoltaic (PV) panel, an MT, and a storage battery (SB).

However, the installation location and capacity of DG and the allocation capacity of various DGs in multienergy networks will have a great impact on the operating technical indicators and economic indicators of the system. Therefore, it is of great importance and necessity to study the optimal allocation of DG in multienergy networks. At present, a lot of researches have been carried out

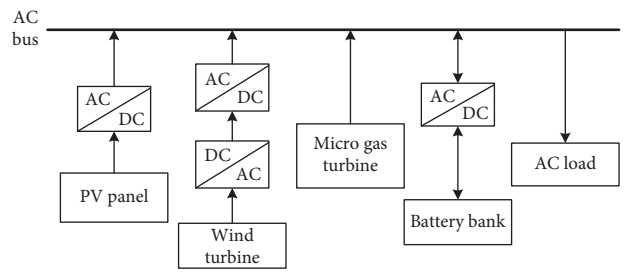

Figure 1: Multienergy network node architecture.

on the optimal allocation of DGs for multienergy networks at home and abroad. For example, literature study [1] adopts a modified particle swarm optimization algorithm to optimize the cost, reliability, and pollutant emissions of hybrid power generation systems. Literature study [2] uses the harmony search algorithm to model and analyze the cost of hybrid systems which include a PV panel, a wind generator (WG), and diesel and then compares them with conventional PV panel/WG/diesel/battery systems. And literature study [3] applies a novel improved fruit fly optimization algorithm-based multiobjective optimization method to optimize the annual total cost and the pollutant emission of the stand-alone hybrid photovoltaic panel-wind generator-diesel-battery system. In addition, literature studies [4–7] have introduced multiobjective optimization algorithms for multiple distributed energy systems. With economic and environmental benefits as optimization objectives, different optimization algorithms are used to optimize the DG allocation capacity of multienergy networks. Besides, literature studies [8–10] introduce a specific allocation method of DG, which is aimed at low system loss or high voltage stability and solves the allocation capacity of DG. However, all of the above studies use the single-level multiobjective optimization function to solve the optimal allocation capacity of DG in multienergy networks when the location of DG is determined, while the installation location of DG needs to be determined by other algorithms.

In this paper, firstly, the first-layer optimization objective function of the minimum active power loss and node voltage offset in the multienergy network system is constructed. The multiobjective optimization strategy based on the nondominated sorting genetic algorithm is used to solve the DG location and sizing. Secondly, in view of the power characteristics of various DGs and the optimization results of the first-layer algorithm, the second-layer algorithm takes into account the economic cost, power supply reliability, and environmental benefits and combines the multiobjective nondominated sorting genetic algorithm to optimize the allocation of various DG capacities. Finally, the proposed algorithm is applied to a multienergy network in a certain area. The results show that the operation performance, economy, reliability, and environmental protection of the multienergy network optimized by the double-layer nondominated sorting genetic algorithm are greatly improved.

2. Multiobjective Nondominated Sorting Genetic Algorithms

2.1. Mathematical Description of the Multiobjective Optimization Algorithm. Taking minimizing multiobjective function with constraints as an example, multiobjective optimization problems can be described as follows:

$$\begin{cases} \min f(X) = [f_1(X), f_2(X), \ldots, f_n(X)], \\ g_i(X) \le 0, \quad i = 1, 2, 3, \ldots, \\ h_j(X) = 0, \quad j = 1, 2, 3, \ldots, \end{cases} \tag{1}$$

where $f(X)$ is a vector space with n objective functions, $g_i(X)$ is the ith inequality constraint function, $h_j(X)$ is the jth equation constraint, and $X = (x_1, x_2, \ldots, x_m)$ is a vector space with m decision variables.

2.2. Decision-Making in Multiobjective Optimization. The multiobjective nondominated sorting genetic algorithm is used to obtain a series of discrete solutions [11–13]. How to choose an optimal solution among these discrete points is the key of the multiobjective optimization. In this paper, an optimal scheme selection method based on the geometric distance method is proposed. The central idea is that the geometric distance between the optimal solution and the positive ideal solution is the shortest, while the geometric distance between the optimal solution and the negative ideal solution is the longest. The optimal solution comes from the optimized Pareto frontier. The positive ideal solution refers to the solution that can satisfy the optimality of each objective function. And the negative ideal solution refers to the solution that does not satisfy any objective functions.

The geometric distance d_i^+ of any solution i on the Pareto frontier to the positive ideal solution is calculated as follows:

$$d_i^+ = \sqrt{\sum_{j=1}^{m} \left(S_{ij} - S_j^{p-\text{ideal}}\right)^2}, \tag{2}$$

where m is the number of objective functions, j is the dimension in which it is located, and $S_{ij} - S_j^{p-\text{ideal}}$ is the linear distance of the jth dimension from the solution i to the positive ideal solution.

The geometric distance d_i^- of any solution on the Pareto frontier to the negative ideal solution is calculated as follows:

$$d_i^- = \sqrt{\sum_{j=1}^{m} \left(S_{ij} - S_j^{n-\text{ideal}}\right)^2}, \tag{3}$$

where $S_{ij} - S_j^{n-\text{ideal}}$ refers to the linear distance of the jth dimension between the solution i and the negative ideal solution.

The coefficient ω_i is defined as follows:

$$\omega_i = \frac{d_i^+}{d_i^+ + d_i^-}. \tag{4}$$

The ω_i corresponding to any solutions in the Pareto frontier can be calculated by (1) to (3), and then the solution corresponding to the smallest ω_i is selected, which is the final optimal solution.

3. First layer: Location and Capacity Optimization of DG

3.1. Decision Variables of the First Layer. The rational planning of the DG in the multienergy network can effectively improve the operating performance of the system, so the decision variables of the first layer are the installation location and capacity of the DG.

This paper uses a set of two-dimensional vectors to represent the decision variables of the first layer, namely, the optimal position and optimal capacity of DG, as shown in Table 1.

3.2. Objective Function of the First-Layer Optimization Algorithm. Reasonable DG installation location and capacity configuration can improve power quality and optimize power flow while taking into account economic benefits. Moreover, some studies have testified that unreasonable locations or sizes of DG may result in greater system losses than the ones in the existing network [14]. The multiobjective optimization function should include economic indicators and technical indicators. The economic index of this layer mainly refers to the minimum active power loss of the multienergy network, and the technical index mainly refers to the minimum voltage offset of load nodes. The objective function is as follows (the function that has to be minimized consists of two objectives: one is economical and the other is technical):

$$\begin{cases} \min P_{\text{loss}} = \sum_{k=1}^{N_1} G_{k(i,j)}\left(U_i^2 + U_j^2 - 2U_iU_j\cos\delta_{ij}\right), \\ \min \Delta U = \sum_{i=1}^{N_d}\left(\dfrac{U_i - U_i^{\text{spec}}}{\Delta U_i^{\max}}\right)^2, \end{cases} \tag{5}$$

where P_{loss} is the active power loss of the multienergy network; ΔU is the offset of the load node voltage in the multienergy network; N_1 represents the number of branches of the multienergy network; N_d represents the number of nodes; $G_{k(i,j)}$ represents the conductance of the branch k (i and j are the node numbers at both ends of the branch k); U_i and U_j represent the voltage amplitudes of the nodes i and j, respectively; δ_{ij} refers to the phase angle difference of the nodes i and j; U_i^{spec} is the desired voltage value of the node i; and $\Delta U_i^{\max}$ is the maximum allowable voltage deviation of the node i, i.e., $\Delta U_i^{\max} = U_i^{\max} - U_i^{\min}$.

3.3. Constraints of the First-Layer Optimization Algorithm. In multienergy networks, constraints are divided into equality constraints and inequality constraints.

Equality constraints are mainly network power flow balancing. Equality constraints of the node i are as follows:

Table 1: Decision variables.

Unit 1		Unit 2		...	Unit n	
Position	Capacity	Position	Capacity	...	Position	Capacity

$$\begin{cases} P_{Gi} + P_{DGi} - P_{Li} - U_i\sum_{j=1}^{N_d} U_j\left(G_{ij}\cos\delta_{ij} + B_{ij}\sin\delta_{ij}\right) = 0, \\ Q_{Gi} - Q_{Li} - U_i\sum_{j=1}^{N_d} U_j\left(G_{ij}\sin\delta_{ij} + B_{ij}\cos\delta_{ij}\right) = 0, \end{cases} \tag{6}$$

where P_{Gi}, P_{DGi}, and P_{Li} refer to the active power of the generator, DG, and load of the node i, respectively; G_{ij} and B_{ij} represent the conductance and admittance between nodes i and j, respectively; and Q_{Gi} and Q_{Li} represent the reactive power of the generator and load of the node i, respectively.

Inequality constraints mainly include the following aspects:

(1) Node voltage constraints:

$$V_{i\min} \le V_i \le V_{i\max}, \quad i = 1, 2, \ldots, N_d, \tag{7}$$

where $V_{i\min}$ and $V_{i\max}$ are the upper and lower limits of the voltage of the node i, respectively.

(2) DG active power upper-limit constraints:

$$0 \le P_{DGi} \le P_{DG\max}, \quad i = 1, 2, \ldots, N_{DG}, \tag{8}$$

where $P_{DG\max}$ is the upper limit of the DG active power and N_{DG} is the number of DGs.

(3) Branch transmission power constraints:

$$|P_k| \le P_{k\max}, \quad k = 1, 2, \ldots, N_1, \tag{9}$$

where $P_{k\max}$ is the upper limit of the transmission power of the branch k.

4. Second Layer: Optimal Capacity Allocation for Various Types of DGs

4.1. DG Modeling. Multienergy networks generally include a WTG, a PV panel, an MT, and an SB [15]. This section establishes power models for various distributed power sources at first.

4.1.1. WTGs. Because of the volatility of wind resources, the power output from the WTG is also unstable. According to the working principle of the WTG, when the wind speed is less than the cut-in wind speed, the WTG does not generate electricity; when the wind speed is greater than the cut-in wind speed and less than the rated wind speed, the WTG generates electricity, and the output electric power varies with the wind speed; when the wind speed is greater than the rated wind speed and less than the cut-out wind speed, the WTG outputs rated power; when the wind speed is greater

than the cut-out wind speed, the WTG stops working and does not generate electricity [16].

The output $P_{\text{wind}}(t)$ of the WTG at time t is as follows [17]:

$$P_{\text{wind}}(t) = \begin{cases} 0, & v(t) \le v_{\text{in}} \text{ or } v(t) \ge v_{\text{out}}, \\ \dfrac{v(t)^3 - v_{\text{in}}^3}{v_{\text{r}}^3 - v(t)^3} * P_{\text{r}}, & v_{\text{in}} \le v(t) \le v_{\text{r}}, \\ P_{\text{r}}, & v_{\text{r}} \le v(t) \le v_{\text{out}}, \end{cases} \tag{10}$$

where $v(t)$ represents the wind speed at time t; v_{in}, v_{r}, and v_{out} represent the cut-in wind speed, the rated wind speed, and the cut-out wind speed, respectively; and P_{r} refers to the rated power of the WTG.

4.1.2. PV Panels. The output voltage and current of the PV panel vary with the change of the illumination intensity and the junction temperature of the battery. They have strong nonlinear characteristics, and there is one maximum power output point under certain working conditions. In order to make full use of solar energy for PV cells, it is necessary to make the working point of PV cells fall at the maximum power point when the illumination intensity and temperature change. Under the maximum power mode, the expressions of power $P_{\text{PV}}(t)$, voltage $V_{\text{PV}}(t)$, and current $I_{\text{PV}}(t)$, that is, the optimum working point t of the PV cell, are as follows [18]:

$$\begin{aligned} P_{\text{PV}}(t) &= V_{\text{PV}}(t) * I_{\text{PV}}(t), \\ V_{\text{PV}}(t) &= V_{\text{mp}} * \left[1 + 0.0539 * \log\left(\frac{H_{\text{T}}(t)}{1000}\right)\right] + \beta * \Delta T(t), \\ I_{\text{PV}}(t) &= I_{\text{SC}} * \left\{1 - a * \left[\exp\left(\frac{V_{\text{PV}}(t) - \Delta V(t)}{b * V_{\text{OC}}}\right) - 1\right]\right\} + \Delta I(t), \\ a &= \left(1 - \frac{I_{\text{mp}}}{I_{\text{SC}}}\right) * \exp\left[\frac{-V_{\text{mp}}}{b * V_{\text{OC}}}\right], \\ b &= \frac{\left(V_{\text{mp}}/V_{\text{OC}}\right) - 1}{\ln\left(1 - \left(I_{\text{mp}}/I_{\text{SC}}\right)\right)}, \\ \Delta T(t) &= T_{\text{A}}(t) + 0.02 * H_{\text{T}}(t) - 25, \\ \Delta V(t) &= V_{\text{PV}}(t) - V_{\text{mp}}, \\ \Delta I(t) &= \alpha * \left(\frac{H_{\text{T}}(t)}{1000}\right) * \Delta T(t) + \left(\frac{H_{\text{T}}(t)}{1000} - 1\right) * I_{\text{SC}}, \end{aligned} \tag{11}$$

where V_{mp} and I_{mp} represent the maximum power point voltage and current of the PV cell, respectively; V_{OC} represents the open circuit voltage; I_{SC} represents the short circuit current; $H_{\text{T}}(t)$ represents the illumination radiance at time t; α represents the current temperature coefficient of the PV cell module; β represents the voltage temperature coefficient of the PV cell module; and $T_{\text{A}}(t)$ represents the ambient temperature at time t.

4.1.3. MTs. MTs are widely used in distributed systems because of their high reliability, long service life, low environmental pollution, and flexible control. Their working principle is that natural gas and high-pressure gas are mixed and burned in the combustion chamber to produce high-quality gas that drives compressors and generators to generate heat and electricity. Suppose that a certain type of MT is operating under full operating conditions and that the electric load is supplied while satisfying the user's cooling and heating load demands. The output power of the MT at time t is as follows [19]:

$$P_{\text{MT}}(t) = \rho * V_{\text{in}}(t) * \text{LH} + C_{\text{P}} * \rho * V_{\text{in}}(t) * \left(T_2(t) - T_1(t)\right), \tag{12}$$

where $P_{\text{MT}}(t)$ represents the power output of the MT at time t, $V_{\text{in}}(t)$ represents the fuel intake amount at time t, ρ is the gas density, LH is the low heating value, C_{P} represents the specific heat capacity, and $T_1(t)$ and $T_2(t)$ indicate the intake air temperature and exhaust gas temperature of the fuel at time t, respectively.

4.1.4. SBs. The SB can suppress the fluctuation of distributed power supply, has the performance of peak shaving and valley filling, and maintains power stability. The output power of the SB is closely related to the operation status of the system [20].

Assuming that lead-acid batteries are used, the state of time t is related to the state of time $t-1$ and the supply and demand of electricity from time $t-1$ to time t. When the total output power of the DG is greater than the load power consumption, the battery pack is in a charging state; otherwise, the battery pack is in a discharging state. The charge of the battery pack at time t can be expressed as follows [19]:

$$P_{\text{SB}}(t) = \begin{cases} P_{\text{SB}}(t-1) + \left(P_{\text{total}}(t) - \dfrac{P_{\text{load}}(t)}{\eta_{\text{inv}}}\right) * \eta_{\text{charge}}; & \text{charge}, \\ P_{\text{SB}}(t-1) - \dfrac{\left(\left(P_{\text{load}}(t)/\eta_{\text{inv}}\right) - P_{\text{total}}(t)\right)}{\eta_{\text{discharge}}}; & \text{discharge}, \end{cases} \tag{13}$$

where $P_{\text{total}}(t) = P_{\text{wind}}(t) + P_{\text{PV}}(t) + P_{\text{MT}}(t)$, $P_{\text{SB}}(t)$ represents the amount of electricity stored in the SB at time t, $P_{\text{total}}(t)$ is the amount of electricity supplied by the DG in the multienergy network at time t, $P_{\text{load}}(t)$ is the load of the system at time t, η_{inv} represents the conversion efficiency of the inverter, η_{charge} is the charging efficiency of the SB, and $\eta_{\text{discharge}}$ is the discharging efficiency of the SB.

4.2. Decision Variables of the Second Layer. The multiobjective optimization algorithm of the first-layer multienergy network has obtained the distributed power supply installation location and total capacity. But the construction

cost, operation cost, output stability, and environmental impact of different types of distributed power supplies are different, so it is necessary to carry out the second-layer multiobjective optimization to obtain the optimal capacity allocation of various distributed power sources.

The main decision variables at the second layer of the network are as follows:

$$X = \{N_{\text{wind}}, N_{\text{PV}}, N_{\text{MT}}, N_{\text{SB}}\}, \tag{14}$$

where $N_{\text{wind}}, N_{\text{PV}}, N_{\text{MT}}$, and N_{SB} represent the number of WTGs, PV cells, MTs, and SBs, respectively.

4.3. Objective Function of the Second-Layer Optimization Algorithm. The objectives of the second-layer optimization algorithm are mainly to consider economy, power supply reliability, and environmental protection. The objective functions are as follows.

4.3.1. Economy. The economy of the multienergy network is mainly reflected by the construction cost and operation cost of the DG system [21]. The objective functions of the economy are as follows:

$$\begin{aligned}
\min C_{\text{total}} &= \min\left(C_{\text{Cpt}} + C_{\text{Mtn}}\right),\\
C_{\text{Cpt}} &= C_{\text{Cpt}}^{\text{wind}} + C_{\text{Cpt}}^{\text{PV}} + C_{\text{Cpt}}^{\text{MT}} + C_{\text{Cpt}}^{\text{SB}},\\
C_{\text{Cpt}}^{\text{wind}} &= N_{\text{wind}} * e_{\text{wind}} * P_{\text{wind}} * \frac{r * (1+r)^{m_{\text{wind}}}}{(1+r)^{m_{\text{wind}}} - 1},\\
C_{\text{Cpt}}^{\text{PV}} &= N_{\text{PV}} * e_{\text{PV}} * P_{\text{PV}} * \frac{r * (1+r)^{m_{\text{PV}}}}{(1+r)^{m_{\text{PV}}} - 1},\\
C_{\text{Cpt}}^{\text{MT}} &= N_{\text{MT}} * e_{\text{MT}} * P_{\text{MT}} * \frac{r * (1+r)^{m_{\text{MT}}}}{(1+r)^{m_{\text{MT}}} - 1},\\
C_{\text{Cpt}}^{\text{SB}} &= * e_{\text{SB}} * P_{\text{SB}} * \frac{r * (1+r)^{m_{\text{SB}}}}{(1+r)^{m_{\text{SB}}} - 1},\\
C_{\text{Mtn}} &= N_{\text{wind}} * \mu(P_{\text{wind}}) + N_{\text{PV}} * \mu(P_{\text{PV}})\\
&\quad + N_{\text{MT}} * \mu(P_{\text{MT}}) + N_{\text{SB}} * \mu(P_{\text{SB}}),
\end{aligned} \tag{15}$$

where C_{total} is the total cost of power generation; C_{Cpt} and C_{Mtn} represent the cost of construction and operation and maintenance of DG in the multienergy network, respectively; $P_{\text{wind}}, P_{\text{PV}}, P_{\text{MT}}$, and P_{SB} represent the output power of each WTG, PV cell, MT, and SB, respectively; $e_{\text{wind}}, e_{\text{PV}}, e_{\text{MT}}$, and e_{SB} represent the unit cost of the WTG, PV cell, MT, and SB, respectively; $\mu(P_{\text{wind}}), \mu(P_{\text{PV}})$, $\mu(P_{\text{MT}})$, and $\mu(P_{\text{SB}})$ represent the operation and maintenance costs of each WTG, PV cell, MT, and SB, respectively; $m_{\text{wind}}, m_{\text{PV}}, m_{\text{MT}}$, and m_{SB} represent the depreciation life of the WTG, PV cell, MT, and SB, respectively; and r is the discount rate of the equipment, generally 8%.

4.3.2. Power Supply Reliability. Multienergy networks contain fluctuating DGs, and the load of multienergy networks also changes with time [22]. Therefore, it is necessary to evaluate the power supply reliability of the system; that is, the rate of load shortage is required. The smaller the rate of power shortage, the higher the reliability of power supply, and vice versa [23]. This paper takes one day ($T = 24$ h) as the period for evaluating the power supply reliability of the system and divides this period into 24 sections. Assuming that the wind speed, light, temperature, and load are constant in each section (1 h), the load shortage rate in one evaluation period of the system is as follows:

$$\begin{aligned}
\min \text{LSRP} &= \sum_{t=1}^{T}\left[\frac{P_{\text{load}}(t) - P_{\text{DG}}(t) * \eta_{\text{inv}}}{P_{\text{load}}(t)} * U(t)\right],\\
P_{\text{DG}}(t) &= N_{\text{wind}} * P_{\text{wind}}(t) + N_{\text{PV}} * P_{\text{PV}}(t) + N_{\text{MT}}\\
&\quad * P_{\text{MT}}(t) + N_{\text{SB}} * \left[P_{\text{SB}}(t) - P_{\text{SB}\min}\right],\\
U(t) &= \begin{cases} 1, & P_{\text{DG}}(t) < P_{\text{load}}(t),\\ 0, & P_{\text{DG}}(t) \geq P_{\text{load}}(t), \end{cases}
\end{aligned} \tag{16}$$

where LSRP represents the one-day load shortage rate of the system; $P_{\text{load}}(t)$ represents the load at time t; $P_{\text{wind}}(t), P_{\text{PV}}(t), P_{\text{MT}}(t)$, and $P_{\text{SB}}(t)$ refer to the output power of the WTG, PV cell, MT, and SB at time t, respectively; $P_{\text{SB}\min}$ represents the minimum residual power allowed by the SB; and η_{inv} represents the efficiency of the inverter.

4.3.3. Environmental Protection. Environmental protection is mainly reflected by the emission of pollutants (NO_x, CO, CO_2, and SO_2) from DGs. WTG power generation and PV power generation belong to clean energy generation, and they do not emit pollutants. Although the output power of the MT can be flexibly controlled, it will emit pollutants. The higher the emission of pollutants, the worse the environmental protection [24]. The environmental cost of power generation EM_{plt} in the evaluation cycle is as follows:

$$\min \text{EM}_{\text{plt}} = \sum_{t=1}^{T}\sum_{i=1}^{n} N_{\text{MT}} * P_{\text{MT}}(t) * (\alpha_i * Q_i), \tag{17}$$

where α_i refers to the i^{th} emission of pollutants of unit power of the MT, Q_i is the treatment fee of i^{th} pollutants of unit power of emission, $P_{\text{MT}}(t)$ denotes the output power of the MT at time t, and N_{MT} is the input quantity of the MT in the system.

4.4. Constraints of the Second-Layer Optimization Algorithm

4.4.1. Power Balance Constraint. In this paper, the DG capacity of the multienergy network solved by the first-layer optimization algorithm is the sum of all kinds of DGs in the second layer so as to ensure the minimum active power loss and voltage offset of the multienergy network. The power constraints are as follows:

$$\left|\frac{\left[P_{\text{DG}}(t) - P_{\text{DG}}^{*}(t)\right]}{P_{\text{DG}}^{*}(t)}\right| \leq \delta(t), \tag{18}$$

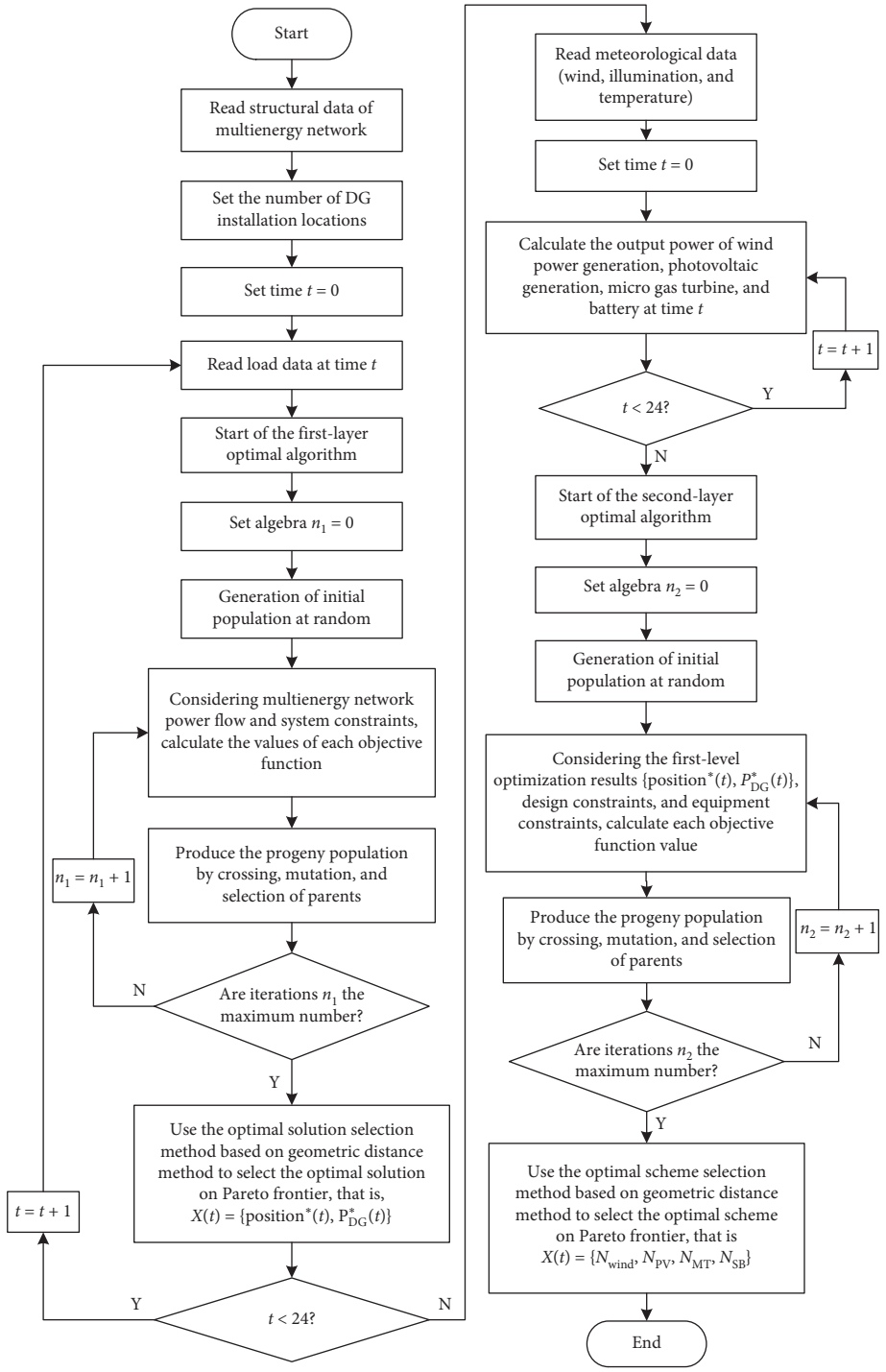

Figure 2: Flow chart of the algorithm.

where $P_{DG}(t) = N_{wind} * P_{wind}(t) + N_{PV} * P_{PV}(t) + N_{MT} * P_{MT}(t) + N_{SB} * P_{SB}(t)$, $P^*_{DG}(t)$ denotes the installed capacity of DGs obtained from the first-layer optimization algorithm at time t, and $\delta(t)$ denotes the maximum unbalanced rate of power that the system can withstand at time t.

4.4.2. Bounds of Design Variables. The bounds of design variables are as follows:

$$\begin{cases} 0 \le N_{wind} \le N^{max}_{wind}, \\ 0 \le N_{PV} \le N^{max}_{PV}, \\ N^{min}_{MT} \le N_{MT} \le N^{max}_{MT}, \\ 0 \le N_{SB} \le N^{max}_{SB}, \end{cases} \tag{19}$$

where N^{max}_{wind}, N^{max}_{PV}, N^{max}_{MT}, and N^{max}_{SB}, respectively, represent the maximum number of WTGs, PV cells, MTs, and SBs that meets the system load demand and N^{min}_{MT} is the minimum

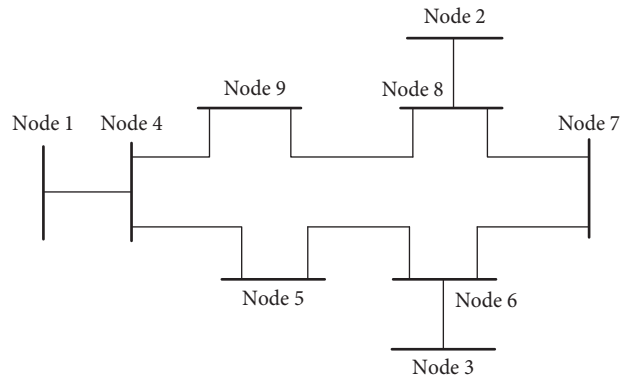

Figure 3: Multienergy network architecture.

number of MTs that meets the condition of "fixing electricity by heat."

4.4.3. Battery Constrains. The battery constraints are as follows:

$$P_{\mathrm{SB\,min}} \le P_{\mathrm{SB}}(t) \le P_{\mathrm{SB\,max}}, \tag{20}$$

where $P_{\mathrm{SB\,max}}$ represents the maximum storage capacity allowed by the SB.

5. Algorithmic Flow

The flow chart of the optimal allocation strategy for the multienergy network based on the double-layer nondominated sorting genetic algorithm proposed in this paper is shown in Figure 2.

6. Case Study

In this paper, a 9-node multienergy network system is taken as an example to verify the optimization effect of the double-layer nondominated sorting genetic algorithm. The topological structure of this multienergy network system is shown in Figure 3. Among them, node 1 is a balanced node, node 3 is a PV node, and the rest nodes are all PQ nodes. The grid parameters (unit values) are shown in Table 2. The evaluation period T of this example is chosen as one day (24 h), and the load data (per unit) and meteorological data in the evaluation period are shown in Figures 4–7 separately. The parameters of lines, WTG, PV panel, MT, and SB and pollutant treatment fee are shown in Tables 2–8, respectively [25].

The optimal allocation strategy proposed in this paper is used to optimize the 9-node multienergy network. The population size of the double-layer optimization algorithm is 200, the number of iterations is 100, and there are two locations in the network where DG can be installed. The first-layer multiobjective optimization algorithm optimizes the location capacity of 24-hour DG in real time based on the 24-hour real-time load data of the network. The second-layer multiobjective optimization algorithm solves the capacity optimization of various DGs with the constraints of the first-layer optimization results, equipment characteristics, and design.

Table 2: Line parameters.

Initial points of the line	End of the line	Resistance	Inductance	Capacitance
1	4	0.000	0.025	0.000
4	5	0.007	0.040	0.017
5	6	0.016	0.073	0.039
3	6	0.000	0.025	0.000
6	7	0.005	0.043	0.023
7	8	0.004	0.031	0.016
8	2	0.000	0.027	0.000
8	9	0.014	0.070	0.033
9	4	0.004	0.037	0.019

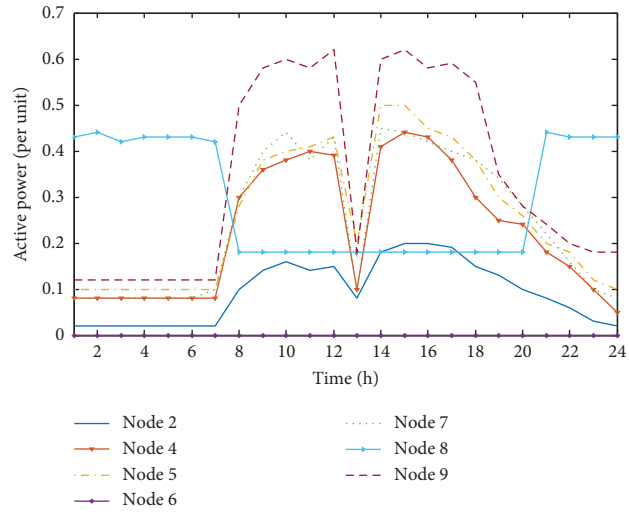

Figure 4: Active power data of the load at each node.

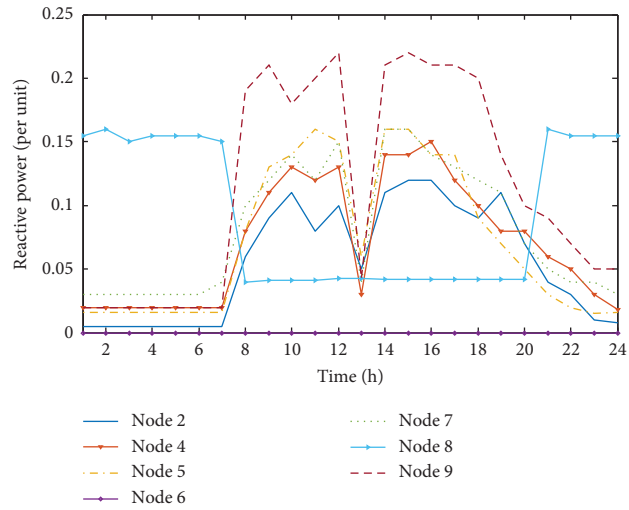

Figure 5: Reactive power data of the load at each node.

The results of the first-layer optimization algorithm are shown in Tables 9 and 10, and the Pareto solution of 100 generations of evolution at a certain time (such as at 13:00) is shown in Figure 8.

The above operation results show that, after adopting the optimal allocation strategy of the multienergy network based

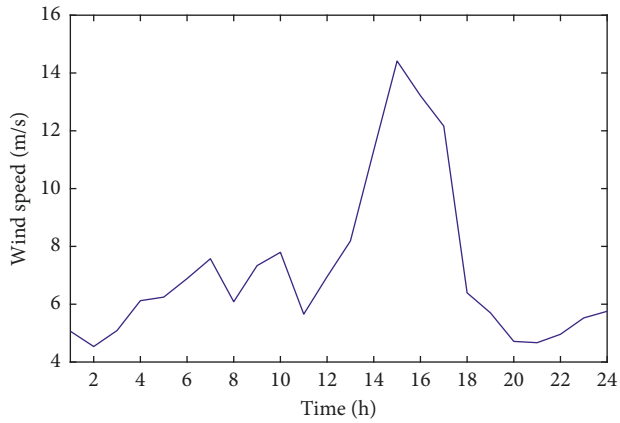

Figure 6: Wind resource data.

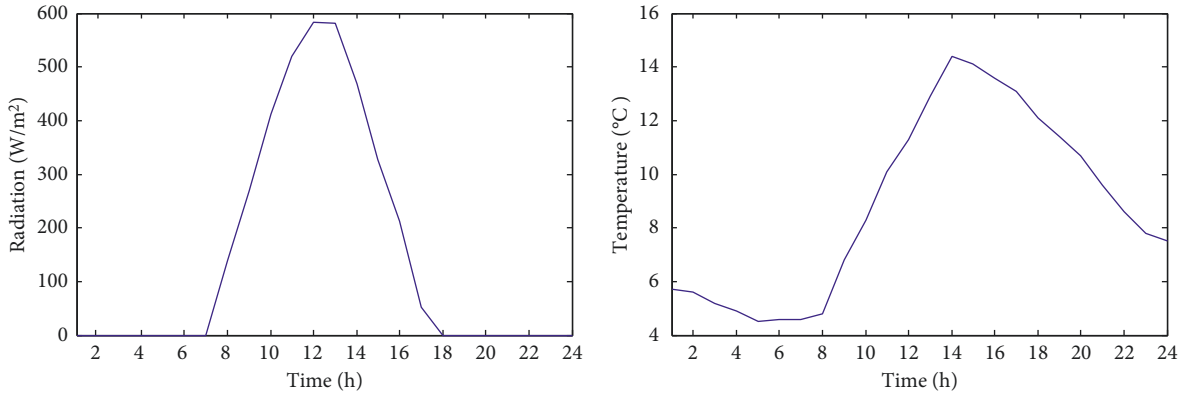

(a) (b)

Figure 7: Solar resource data. (a) Radiation. (b) Temperature.

Table 3: Wind turbine generator parameters.

P_r (kW)	V_{in} (m/s)	V_r (m/s)	V_{out} (m/s)	N_{wind}^{max}
500	3	12	25	8

Table 4: PV panel parameters.

P_r (kW)	V_{OC} (V)	I_{sc} (A)	V_{mp} (V)	I_{mp} (A)	Series number	Parallel number	N_{PV}^{max}
100	64.6	6.14	54.7	5.76	5	64	30

Table 5: MT parameters.

P_r (kW)	C_p (kJ/kg·K)	LH (MJ/m³)	ρ (kg/m³)	T_1 (°C)	T_2 (°C)	N_{MT}^{max}	N_{MT}^{min}
300	2.16	32.6	0.75	25	280	20	1

Table 6: Battery parameters.

P_r (kW)	$P_{SB\,ini}$ (kW)	$P_{SB\,min}$ (kW)	$P_{SB\,max}$ (kW)	η_{charge}	$\eta_{discharge}$	η_{inv}	N_{SB}^{max}
24	9.6	4.8	24	0.85	0.98	0.87	40

Table 7: Cost values.

Type	Life span (years)	Unit cost ($/kW)	Maintenance cost ($/kW)
WTG	20	523	38
PV panel	20	508	29
MT	20	1160	92
SB	10	156	22

Table 8: Pollutant emission of the MT.

Type	NO_x	CO_2	CO	SO_2
Value (g/kWh)	0.6188	184.0829	0.1702	0.000928
Maintenance ($/kg)	0.250	0.00125	0.020	0.125

Table 9: The first-layer decision variables.

Time	First location	First sizing	Second location	Second sizing
1:00	8	0.7587	9	0.2803
2:00	8	0.2184	9	0.8181
3:00	8	0.4325	9	0.5976
4:00	8	0.7628	9	0.2839
5:00	8	0.7074	9	0.3300
6:00	8	0.7541	9	0.2678
7:00	8	0.2695	9	0.7638
8:00	8	0.7190	9	0.7229
9:00	8	0.8485	9	0.7799
10:00	8	0.8922	9	0.7764
11:00	8	0.8608	9	0.8028
12:00	8	0.8887	9	0.8094
13:00	8	0.3797	9	0.4001
14:00	8	0.7833	9	0.9528
15:00	8	0.8063	9	0.9492
16:00	8	0.9274	9	0.7632
17:00	8	0.8883	9	0.7713
18:00	8	0.7370	9	0.8519
19:00	8	0.5159	9	0.7931
20:00	8	0.4600	9	0.7055
21:00	8	0.8561	9	0.3772
22:00	8	0.7965	9	0.3319
23:00	8	0.6882	9	0.3499
24:00	8	0.5463	9	0.4537

Table 10: Comparison of the optimization index.

	System loss ($\times 10^{-3}$)	Voltage deviation
Before optimization	8.435	0.416
After optimization	0.413~5.603	0.015~0.351
Final optimal solution	3.815	0.215

on the double-layer nondominated sorting genetic algorithm, the active power loss of the multienergy network is reduced by 54.77% and the system voltage deviation is reduced by 48.32%. This proves that this strategy can effectively improve the operating conditions of the system, guarantee the stability and economic benefits, and improve the power quality.

The results of the second-layer optimization algorithm are shown in Table 11, and the Pareto solution of the 100-generation evolution is shown in Figure 9. Comparing the optimization solution of this paper with the nonoptimization solution, the results are shown in Table 12. Nonoptimization solution only consists of a single type of DG such as WTG, PV, MT, and SB, and its capacity is capped.

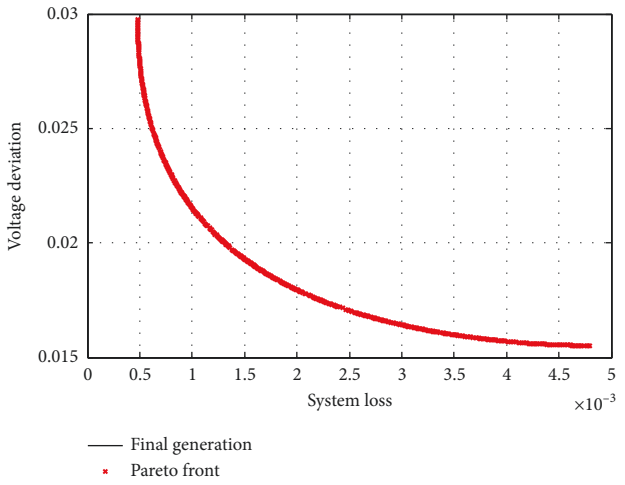

Figure 8: The Pareto front result at 13:00.

Table 11: The second-layer decision variables.

DG location	N_{wind}	N_{PV}	N_{MT}	N_{SB}
First	2	7	17	7
Second	1	8	13	23

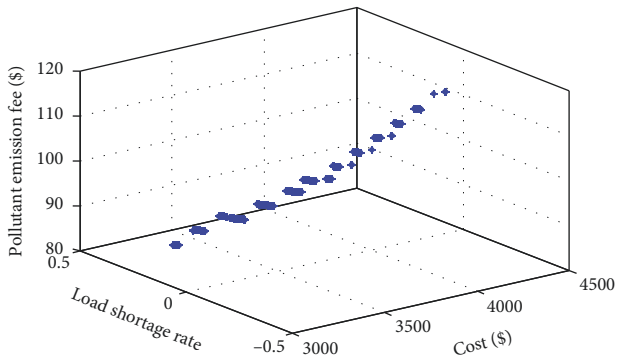

Figure 9: The second Pareto front result.

Table 12: Comparison of the optimization index.

	N_{wind}	N_{PV}	N_{MT}	N_{SB}	C_{total} ($)	LSRP	EM_{plt} ($)
Without optimization	16	0	0	0	949.63	6.64	0.0
	0	60	0	0	561.77	10.24	0.0
	0	0	40	0	2656.32	3.49	111.84
	0	0	0	80	127.96	19.57	0.0
	16	60	40	80	4295.67	0.0	111.84
With optimization	3	15	30	30	3448.83	0.26	81.08

When there are no optimization and only a single type of DG, although the costs of construction, operation, and maintenance are relatively low, the power shortage rate and the cost of pollutant treatment are relatively high. When there are no optimization and all kinds of DGs, although the load power shortage rate is 0, the cost of construction, operation, maintenance, and pollutant treatment is relatively high. Considering the economy, reliability, and environmental protection of the system at the same time, it is necessary to optimize DG allocation of the multienergy network by using the double-layer nondominated sorting genetic algorithm. After optimization, the relative environmental cost and load power shortage rate of the multienergy network are maintained at a relatively low level, which improves the economic effect, environmental protection benefits, and power supply reliability.

7. Conclusion

Aiming at the complex and changeable multienergy network, this paper proposes a multienergy network optimal allocation strategy based on the double-layer nondominated sorting genetic algorithm. Firstly, according to the network load and grid structure, the first-layer optimization algorithm calculates the optimal location and capacity of DG in the multienergy network with the purpose of reducing the network loss and the system voltage offset. Subsequently, the second-layer optimization algorithm takes the first-layer calculation results as constraints and calculates the optimal allocation of different types of DGs, whose purpose is to improve economy, power supply reliability, and environmental protection. The double-layer optimization algorithm uses the optimal scheme selection method based on the geometric distance method to solve the decision variables. Finally, the case study in this paper shows that the double-layer optimal allocation strategy can effectively reduce network loss, improve system voltage, reduce system cost, improve system power supply reliability, increase system environmental benefits, and provide guidance for the design and optimal operation of multienergy networks.

Data Availability

The data used to support the findings of this study are included within the article.

Conflicts of Interest

Min Mou, Da Lin, Yuhao Zhou, Wenguang Zheng, Jiongming Ruan, and Dongdong Ke are employees of Huadian Electric Power Research Institute Co., Ltd., Hangzhou, Zhejiang 310013, China.

Acknowledgments

This work was supported by the National Key R&D Program of China under No. 2018YFB0905101.

References

[1] L. Wang and C. Singh, "Multicriteria design of hybrid power generation systems based on a modified particle swarm optimization algorithm," *IEEE Transaction on Energy Conversion*, vol. 24, no. 1, pp. 163–172, 2009.

[2] A. Maleki and F. Pourfayaz, "Sizing of stand-alone photovoltaic/wind/diesel system with battery and fuel cell storage devices by harmony search algorithm," *Journal of Energy Storage*, vol. 2, pp. 30–42, 2015.

[3] J. Zhao and X. Yuan, "Multi-objective optimization of stand-alone hybrid PV-wind-diesel-battery system using improved fruit fly optimization algorithm," *Soft Computing*, vol. 20, no. 7, pp. 2841–2853, 2016.

[4] Y.-Y. Hong and R.-C. Lian, "Optimal sizing of hybrid wind/PV/diesel generation in a stand-alone power system using Markov-based genetic algorithm," *IEEE Transactions on Power Delivery*, vol. 27, no. 2, pp. 640–647, 2012.

[5] M. A. Abido, "Environmental/economic power dispatch using multiobjective evolutionary algorithms," *IEEE Transactions on Power Systems*, vol. 18, no. 4, pp. 1529–1537, 2003.

[6] Q. Lin, J. Chen, Z. Zhan et al., "A hybrid evolutionary immune algorithm for multiobjective optimization problems," *IEEE Transaction on Evolutionary Computation*, vol. 20, no. 5, pp. 711–728, 2016.

[7] W. Kellogg, M. H. Nehrir, G. Venkataramanan, and V. Gerez, "Optimal unit sizing for a hybrid wind/photovoltaic generating system," *Electric Power Systems Research*, vol. 39, no. 1, pp. 35–38, 1996.

[8] M. Gandomkar, M. Vakilian, and M. Ehsan, "A genetic-based Tabu search algorithm for optimal DG allocation in distribution networks," *Electric Power Components and Systems*, vol. 33, no. 12, pp. 1351–1362, 2005.

[9] C. L. T. Borges and D. M. Falcão, "Optimal distributed generation allocation for reliability, losses, and voltage improvement," *International Journal of Electrical Power & Energy Systems*, vol. 28, no. 6, pp. 413–420, 2006.

[10] A. Kazemi and M. Sadeghi, "Distributed generation allocation for loss reduction and voltage improvement," in *Proceedings of the 2009 Asia-Pacific Power and Energy Engineering Conference*, pp. 518–524, IEEE, Wuhan, China, March 2009.

[11] H. Li and Q. Zhang, "Multiobjective optimization problems with complicated Pareto sets, MOEA/D and NSGA-II," *IEEE Transactions on Evolutionary Computation*, vol. 13, no. 2, pp. 284–302, 2009.

[12] K. Deb, *Multi-Objective Optimization Using Evolutionary Algorithms*, Wiley, New York, NY, USA, 2001.

[13] D. Liu, K. C. Tan, C. K. Goh, and W. K. Ho, "A multiobjective memetic algorithm based on particle swarm optimization," *IEEE Transactions on Systems, Man, and Cybernetics, Part B (Cybernetics)*, vol. 37, no. 1, pp. 42–50, 2007.

[14] T. Griffin, K. Tomsovic, D. Secrest, and A. Law, "Placement of dispersed generations systems for reduced losses," in *Proceedings of the 33rd Annual Hawaii International Conference on System Sciences*, Maui, HI, USA, January 2000.

[15] X. Q. Kong, R. Z. Wang, and X. H. Huang, "Energy optimization model for a CCHP system with available gas turbines," *Applied Thermal Engineering*, vol. 25, no. 2-3, pp. 377–391, 2005.

[16] F. Cheng, L. Qu, W. Qiao, C. Wei, and L. Hao, "Fault diagnosis of wind turbine gearboxes based on DFIG stator current envelope analysis," *IEEE Transactions on Sustainable Energy*, vol. 10, no. 3, pp. 1044–1053, 2019.

[17] Y. Z. Sun, J. Wu, G. J. Li, and J. He, "Dynamic economic dispatch considering wind power penetration based on wind speed forecasting and stochastic programming," *Proceedings of the CSEE*, vol. 29, no. 4, pp. 41–47, 2009.

[18] B. S. Borowy and Z. M. Salameh, "Methodology for optimally sizing the combination of a battery bank and PV array in a wind/PV hybrid system," *IEEE Transactions on Energy Conversion*, vol. 11, no. 2, pp. 367–375, 1996.

[19] R. Wang, *Research on Multi-Objective Optimization Design and Coordinated Control of Distributed Generation and Microgrid*, Shandong University, Jinan, China, 2013.

[20] C. Wei, M. Benosman, and T. Kim, "Online parameter identification for state of power prediction of lithium-ion batteries in electric vehicles using extremum seeking," *International Journal of Control, Automation and Systems*, 2019.

[21] W. El-Khattam, K. Bhattacharya, Y. Hegazy, and M. M. A. Salama, "Optimal investment planning for distributed generation in a competitive electricity market," *IEEE Transaction on Power System*, vol. 19, no. 3, pp. 1674–1684, 2004.

[22] D. Singh, D. Singh, and K. S. Verma, "Multiobjective optimization for DG planning with load models," *IEEE Transaction on Power System*, vol. 24, no. 1, pp. 427–436, 2009.

[23] A. A. Chowdhury, S. K. Agarwal, and D. O. Koval, "Reliability modeling of distributed generation in conventional distribution systems planning and analysis," *IEEE Transaction on Industry Application*, vol. 39, no. 5, pp. 1493–1498, 2003.

[24] M. Abido, "Environment/economic power dispatch using multiobjective evolutionary algorithm," *IEEE Transaction on Power System*, vol. 18, no. 4, pp. 1529–1537, 2003.

[25] W. D. Kellogg, M. H. Nehrir, G. Venkataramanan, and V. Gerez, "Generation unit sizing and cost analysis for stand-alone wind, photovoltaic, and hybrid wind/PV systems," *IEEE Transactions on Energy Conversion*, vol. 13, no. 1, pp. 70–75, 1998.